Biochemical and Biophysical Research Communications 393 (2010) 734–739

Contents lists available at ScienceDirect

Biochemical and Biophysical Research Communications

journal homepage: www.elsevier.com/locate/ybbrc

Arabidopsis dynamin-related protein 1A polymers bind, but do not tubulate, liposomes

Steven K. Backues, Sebastian Y. Bednarek *

Department of Biochemistry, University of Wisconsin – Madison, 433 Babcock Dr., Madison, WI 53706, USA

ARTICLE INFO

Article history:
Received 6 February 2010
Available online 18 February 2010

Keywords:
Arabidopsis
DRP1A
Dynamin
GTPase
Liposome flotation
Spotted lipid overlay

ABSTRACT

The *Arabidopsis* dynamin-related protein 1A (*At*DRP1A) is involved in endocytosis and cell plate maturation in *Arabidopsis*. Unlike dynamin, *At*DRP1A does not have any recognized membrane binding or protein–protein interaction domains. We report that GTPase active *At*DRP1A purified from *Escherichia coli* as a fusion to maltose binding protein forms homopolymers visible by negative staining electron microscopy. These polymers interact with protein-free liposomes whose lipid composition mimics that of the inner leaflet of the *Arabidopsis* plasma membrane, suggesting that lipid-binding may play a role in *At*DRP1A function. However, *At*DRP1A polymers do not appear to assemble and disassemble in a dynamic fashion and do not have the ability to tubulate liposomes *in vitro*, suggesting that additional factors or modifications are necessary for *At*DRP1A's *in vivo* function.

Introduction

The *Arabidopsis* dynamin-related protein 1A (*At*DRP1A) is a member of the dynamin superfamily of GTPases that plays a critical role in *Arabidopsis* development [1–5]. It is essential for proper maturation of the cell plate during cytokinesis [3,4,6], and recent studies have also suggested that it functions like dynamin in Clathrin-Mediated Endocytosis (CME) [5]. Dynamin is the founding and best characterized member of the dynamin superfamily, and plays both early regulatory and late mechanical roles in the formation and severing of clathrin-coated vesicles from the plasma membrane (PM)[7]. During CME, dynamin activity at endocytic buds is regulated by a combination of its pleckstrin homology (PH) domain, which binds the signaling phospholipid $PI(4,5)P_2$, and its proline rich domain (PRD), which binds other endocytic proteins. Neither of these domains, nor any other recognized lipid- or protein-binding domains, are present in *At*DRP1A, raising the question of how *At*DRP1A is targeted and regulated during endocytosis and cytokinesis.

Subcellular fractionation studies have revealed that *At*DRP1A is a peripheral membrane protein that is predominantly present as a high molecular weight protein complex [3,8]. However, it has not been determined whether *At*DRP1A binds directly to membranes or indirectly via other protein partners, and whether the high molecular weight complexes are homopolymers of *At*DRP1A or multi-protein complexes. The soybean homolog of *At*DRP1A, *Gm*DRP1 (Phragmoplastin), was reported to form a homopolymer when purified from *E. coli* as a glutathione-S-transferase (GST) fusion protein, and two self-interaction domains were identified by yeast-two-hybrid and *in vitro* binding studies [9]. However, GST-*Gm*DRP1 was purified under denaturing conditions, and was not demonstrated to have GTPase activity, limiting its utility for biochemical characterization.

Here we present the *in vitro* characterization of GTPase active, *E. coli* expressed, *At*DRP1A, including evidence of its inherent self-interaction and lipid-binding ability. Significantly, purified *At*DRP1A behaves very differently than purified dynamin, and in ways that are difficult to reconcile with what is known of its *in vivo* activity, suggesting that additional factors or modifications are needed for *At*DRP1A to function.

Materials and methods

General reagents. All reagents were purchased through Fisher Scientific (Pittsburg, PA) unless otherwise noted. SDS–PAGE and immunoblotting conditions and α-DRP1A antibodies are described in [3] with the exception that Supersignal West Pico (Pierce,

Abbreviations: *At*DRP1A, *Arabidopsis* dynamin-related protein 1A; CME, clathrin-mediated-endocytosis; DOPC, dioleoyl-phosphatidyl choline; DOPE, dioleoyl-phosphatidyl ethanolamine; DOPG, dioleoyl-phosphatidyl glycerol; DOPS, dioleoyl-phosphatidyl serine; EM, negative staining electron microscopy; MBP, maltose binding protein; PM, plasma membrane; PMM, plasma membrane mimetic; PH, pleckstrin homology; PIP, phosphatidyl inositol phosphate; PRD, proline rich domain; Soy PC, soybean phosphatidyl choline; TEV, Tobacco-Etch-virus protease.

* Corresponding author. Fax: +1 608 262 3453.
E-mail address: sybednar@wisc.edu (S.Y. Bednarek).

0006-291X/$ - see front matter © 2010 Elsevier Inc. All rights reserved.
doi:10.1016/j.bbrc.2010.02.070

Rockford, IL) was used as the chemiluminesence substrate for detection of the HRP-labeled secondary antibodies. Rabbit α-MBP antibodies were purchased from Immunology Consultants Laboratories (Newberg, OR). Spotted lipid assays were performed as described by Dowler et al. [10]. All oligonucleotides were purchased from Integrated DNA Technologies (Coralville, IA) and PCR amplification was performed with PfuUltra (Stratagene, La Jolla, CA).

Generation of the His_8-MBP-AtDRP1A expression clone. The *At*DRP1A coding sequence (full length, including stop codon) was PCR amplified using primers 5′-ggggacaagtttgtacaaaaaagcaggctcaatg gaaaatctgatctctctggttaa-3′ (forward) and 5′-ggggaccactttgtacaaga aagctgggtatcacttggaccaagcaacagcatcgatctcg-3′ (reverse), which introduced attB1/B2 recombination sites at the ends of the gene. The PCR product was inserted into the plasmid pGEM-T-EASY (Promega, Madison WI) by TA cloning and then recombined into pDONR201 (Invitrogen, Carlsbad, CA) using standard Gateway® cloning procedures (Invitrogen, Carlsbad, CA). A DNA sequence encoding the Tobacco-Etch Virus (TEV) cleavage site was inserted in frame with the first codon of DRP1A by site-directed mutagenesis [11] using the 5′ phosphorylated primers 5′-gagaacctctattt ccagggcgaaaatctgatctctctggttaac-3′ and 5′-tgagcctgctttttttgtacaaag-3′, which annealed to *At*DRP1A and pDONR201, respectively. The *At*DRP1A coding sequence was verified by sequencing, and then recombined into the destination vector pVP16 [12] to created pVP16-TEV-DRP1A. pVP16 contains His_8-Maltose Binding Protein (His_8-MBP), in frame with the N-terminus of the gene inserted into the recombination site (e.g., TEV-DRP1A).*Expression and purification of DRP1A*. pVP16-TEV-DRP1A in *E. coli* strain B834pRARE2 was used to inoculate 50 mL of LB (Luria Broth + carbenicillin$^{50\ \mu g/ml}$/chloramphenicol$^{34\ \mu g/ml}$) which was grown to saturation (16 h) with shaking at 37 °C. This culture was diluted 1:20 into 1 L LB and immediately induced with 1 mM Isopropyl β-D-1-thiogalactopyranoside (IPTG). The 1 L culture was grown an additional 16 h with shaking at 18 °C. The bacteria expressing His_8-MBP-TEV-DRP1A were harvested by centrifugation (10 min at 2000*g*) and resuspended in 10 ml H(0.15)NG buffer (25 mM HEPES pH 7.5, 0.15 M NaCl, 5% v/v glycerol, 10 mM β-ME) with protease inhibitors and 1 mg/ml lysozyme prior to lysis by French Press (2 passes, 1900 PSI). The lysis mixture was cleared twice by centrifugation at 2000*g* and TX-100 was added to the supernatant to a final concentration of 2% (v/v) before incubation with 1 ml bed volume amylose resin (New England Biolabs, Ipswich, MA) in a 10 ml disposable poly-prep column (Biorad, Hercules, CA) at 4 °C with rotation for ⩾ 30 min. The unbound was drained by gravity flow and the resin washed with 10mls H(0.15)NG + 1 mM ATP + 2%TX-100 and then 50 ml cold H(0.15)NG prior to elution with H(0.15)NG + 10 mM maltose. The concentration of purified His_8-MBP-TEV-DRP1A was measured with Biorad protein assay reagent (Biorad, Hurcules, CA) and diluted to 0.5 mg/ml (5 mM). Purified His_6-TEV protease [12] was added to a concentration of 0.25 mg/ml and the cleavage reaction was incubated with rotation at 22 °C for 24–48 h. Purity of the preparation and completeness of the cleavage reaction was assayed by SDS–PAGE. Cleaved *At*DRP1A was frozen in liquid nitrogen and stored at −80 °C.

GTPase assays. Colorimetric GTPase assays for determination of kCAT and kM were performed essentially as described by Leonard et al. [13]. In brief, purified *At*DRP1A (0.1 μM final) was mixed with GTP (50–500 μM final) in reaction buffer (20 mM HEPES, pH 7.5, 150 mM NaCl, 2 mM $MgCl_2$) and incubated at 22 °C; 0, 2, 5, 10 and 15 min time points were taken and concentrations of released phosphate determined by addition of the color reagent (1 M HCl, 0.1% w/v Malachite Green, 1% w/v Ammonium Molybdate Tetrahydrate) and measurement of absorbance at 660 nM on a plate reader (Bio-Tek instruments EL311).

Fractionation. Purified His_8-MBP-*At*DRP1A or *At*DRP1A was diluted to 200 nM in H(0.15)NG + 2 mM $MgCl_2$ with or without 1 mM GTP and incubated 5 min 22 °C. After 5 min, an additional 1 mM GTP was added to the + GTP sample, and 200 μl of each sample was transferred to a TLA100.1 tube and pelleted for 30 min at 150,000*g* in a Beckman (Fullerton, CA) tabletop ultracentrifuge. The load and upper 80 μl of the reaction volume were analyzed by SDS–PAGE and immunoblotting against *At*DRP1A and MBP. For sucrose gradient fractionation, 200 μl of 1.25 μM *At*DRP1A was loaded on top of a 4.8 mL 5–50% (w/v) sucrose gradient in H(0.075)N (25 mM HEPES pH 7.5 m, 0.075 M NaCl, 2 mM $MgCl_2$, and 10 mM β-ME) poured on an Autodensiflow gradient maker (Labconco, Kansas City, Kansas). Gradients were centrifuged 18 h at 4 °C in a SW50.1 rotor at 150,000*g*. 200 μl fractions were collected using a gradient collector (model 640, Isco Inc., Lincoln, NE). Fractionation standards (75 μg BSA, 75 μg Catalase, 50 μg *At*CDC48 [14]), were loaded on an identical gradient and centrifuged and fractionated in parallel. The fractions were analyzed by SDS PAGE followed by Coomassie staining (fractionation standards) or immunoblotting using α-*At*DRP1A antibodies, and refractive index was used to compare fractions between gradients.

Liposome generation. DOPC, DOPS, DOPE, Soy PC and PI(4,5)P_2 were purchased from Avanti Polar Lipids (Alabaster, AL). PI(3)P, PI(4)P and PI(5)P were from Cayman Chemical (Ann Arbor, MI), and β-sitosterol was from Calbiochem (San Diego, CA). Dried lipids were resuspended in chloroform or 1:1 chloroform/methanol and mixed by vortexing in a 12 × 75 mm glass test tube. The lipid mixture was spiked with ^{3}H-DOPC (Perkin–Elmer) to 6 μCi/ml and dried under a gentle stream of Argon until visibly dry (10–15 min), and then placed under house vacuum for an additional 30 min. The resulting film was resuspended to 330 mM total lipid in H(0.15NG) buffer and allowed to hydrate 15 min at RT before being vortexed for 5 min. The mixture was then subjected to five free-thaw cycles (liquid nitrogen −37° water bath) before being extruded through a 50 nm polycarbonate membrane (Avanti Polar Lipids, Alabaster, AL) and stored at −80 °C under argon until use.

Liposome flotation assays. Liposome flotation assays were performed generally as described in [15]. Purified *At*DRP1A protein (200 nM to 1 μM final concentration) was mixed with 50 nm liposomes (44 mM final concentration) and buffer H(0.15)NG to a final volume of 75 μl in a sialinized 0.65 ml ultracentrifuge tube and incubated 30 min at 22 °C with occasional mixing. The binding reaction was diluted with an equal volume of ice-cold 80% (w/v) Accudenz (Accurate Chemical and Scientific Corporation, Westbury, NY) in H(0.015)NG, transferred to the bottom of a 5 × 41 mm Ultra-Clear centrifuge tube (Beckman-Coulter), and overlayed with 300 μl 30% (w/v) Accudenz followed by 100 μl H(0.15)NG then centrifuged 1 h or more at 243,000*g* at 4 °C in an SW50.1 rotor with tube adapters. Fractions (80 μl) were collected from the top and analyzed for lipid content by scintillation counting and protein content by SDS–PAGE followed by Coomassie staining or immunoblotting.

Negative staining electron microscopy. All electron microscopy was performed at the UW Madison Medical School EM Facility on a Phillips CM120 STEM. For visualization of *At*DRP1A, purified protein was diluted to 1 μM in buffer H(0.075)N with or without 1 mM GTP, dried onto a pioloform (Ted Pella, Redding, CA) coated copper grid, and stained with Nano-W® (Nanoprobes, Yaphank, NY), an organo-tungstate stain. Liposomes were diluted to 100 mM lipid in H(0.075)N, mixed with an equal volume 1% OsO_4, then dried onto pioloform coated grids and stained with Nano-W®. For visualization of *At*DRP1A bound to liposomes, purified *At*DRP1A was mixed with liposomes to a final concentration of 1 μM *At*DPR1A and 100 mM lipid in H(0.075)N and incubated for 30 min 22 °C with occasional mixing. The mixture was then stained with OsO_4 and Nano-W® as for liposomes.

Results and discussion

Purification of GTPase active AtDRP1A

GTPase active *At*DRP1A was expressed in *E. coli* as a translational fusion to a His_8-MBP tag, purified using amylose affinity chromatography and treated with His_6-TEV protease to remove the His_8-MBP tag (Fig. 1A). The GTPase activity of the purified protein increased approximately twofold upon cleavage of the His_8-MBP tag (Fig. 1B). In contrast, expression of other affinity tagged forms of *At*DRP1A, including GST-*At*DRP1A in *E. coli* and *S. cerevisae* and *At*DRP1A-His_6 in *S. cerevisae*, did not yield GTPase-active protein.

His_8-MBP and His_6-TEV protease could not be removed from the mixture by immobilized Ni affinity chromatography due to non-specific binding of *At*DRP1A to the nickel resin. Therefore, in all subsequent experiments, *At*DRP1A was assayed in the presence of cleaved His_8-MBP and His_6-TEV, with a mixture of His_6-TEV and purified His_8-MBP serving as a negative control.

The kCat and kM of GTP hydrolysis by *At*DRP1A was measured by a colorimetric GTPase assay [13] in the presence of varying concentrations of GTP (Fig. 1C). k_{cat} and k_M values varied between preparations, as has been observed for dynamin [16]. The average k_{cat} value was 28 ± 5.34/min, which falls between the k_{cat} values reported for lipid-tubule stimulated (105 ± 47/min) and unstimulated dynamin (2.6 ± 0.98/min) [17]. The average k_M was 99 ± 59 μM, which is lower than that reported for stimulated (37 ± 18 μM), but similar to that of unstimulated (102 ± 35 μM) dynamin [17].

Purified AtDRP1A is polymeric

As shown in Fig. 1A, His_8-MBP-DRP1A, *At*DRP1A, and His_8-MBP migrated as 110 kD, 65 kD and 45 kD polypeptides, respectively, when analyzed by SDS–PAGE. However, when the *At*DRP1A cleavage mixture, containing *At*DRP1A, His_8-MBP and His_6-TEV, was subjected to centrifugation at 150,000*g*, *At*DRP1A, but not His_8-MBP, was fully depleted from the supernatant (Fig. 2A). His_8-MBP-*At*DRP1A likewise pelleted at 150,000*g*, indicating that both His_8-MBP tagged and tag-free *At*DRP1A form large homopolymers in the presence of 150 mM NaCl. This sedimentation behavior was not altered by incubation with 1 mM GTP (Fig. 2A). When subjected to velocity sedimentation gradient analysis in the presence of 75 mM NaCl, *At*DRP1A sedimented beneath the 17S/550 kDa protein standard, CDC48 [14], further demonstrating the polymeric nature of *E. coli* expressed *At*DRP1A (Fig. 2B). This behavior is distinctly different than that of purified dynamin, which is found both in polymeric and soluble, dimeric/tetrameric forms, with the soluble form favored in the presence of ⩾ 25 mM NaCl or upon addition of GTP [18–20].

When purified dynamin is induced to polymerize by dilution into ⩽ 25 mM NaCl buffers or by addition of GDP-BeF_2, it forms rings and spirals with a constant diameter [21,22]. In contrast, the size and shape of tag-free *At*DRP1A polymers visualized by negative staining electron microscopy (EM) was found to be highly heterogeneous, with no discernible regularity in structure (Fig. 2C). Addition of GTP to purified *At*DRP1A did not result in a visible change in polymer size or structure (Supplementary Fig. 1).

Similar to animal dynamin [18] GST-*Gm*DRP1 was reported to exist predominantly as monomers and dimers in the presence of 150 mM NaCl, only forming large polymers with a helical nature at 15 mM NaCl [9]. However, these results were based solely on EM analysis, and were not verified through other analytical methods. The smallest *At*DRP1A particles we observed by EM (Fig. 2C, arrowheads) were similar in appearance to those interpreted as 68 kDa monomers or dimers of GST-*Gm*DRP1 by Zhang et al. [9]; however by analytical sedimentation analysis (Fig. 2B) we estimate these structures to be comprised of more than 10 subunits (i.e., ⩾680 kDa). The larger *At*DRP1A structures we observed at 75 mM NaCl (Fig. 2C, arrows) are similar in appearance to the helical arrays of GST-*Gm*DRP1 imaged by Zhang et al. [9] at 15 mM NaCl. However, the *At*DRP1A structures (Fig. 2C) are heterogenous in size and curvature, and resemble neither the regular polymers formed by purified dynamin [21] nor the 45 nm diameter *At*DRP1A-containing rings observed encircling cell plate membrane tubules during syncytial endosperm cellularization [6].

AtDRP1A interacts with PM-mimetic liposomes

In interphase *Arabidopsis* cells, *At*DRP1A-GFP localizes to endocytic sites at the PM [5], and fractionation studies of cell extracts have similarly shown *At*DRP1A to be primarily associated with microsomal membranes [3,8]. Previous studies have demonstrated that dynamin assembles onto PI(4,5)P_2-containing liposomes via specific interactions between the PI(4,5)P_2 headgroup and dynamin's PH domain, and that this interaction is essential for dyanmin's function in CME [23,24]. However, the *At*DRP1A amino acid sequence does not contain any predicted lipid-binding domains

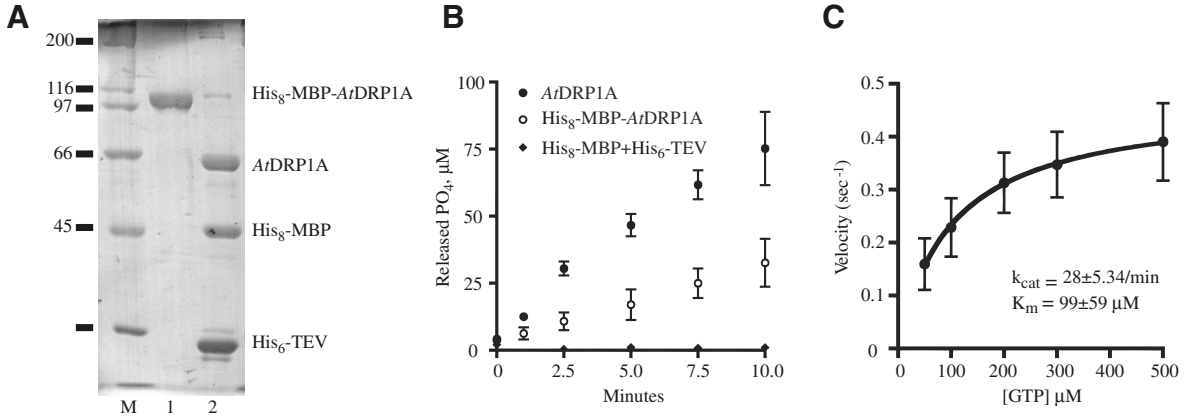

Fig. 1. Production of GTPase active *At*DRP1A. (A) SDS–PAGE gel analysis of *E. coli* expressed, amylose resin purified, His_8-MBP-*At*DRP1A and *At*DRP1A prior to (lane 1) and after (lane 2) cleavage of His_8-MBP with TEV protease. Proteins were detected by Coomassie staining. M = Molecular Mass Standards. (B) The GTPase activity of purified *At*DRP1A, His_8-MBP-AtDRP1A and a mixture of His_8-MBP and His_6-TEV (negative control) was assayed with a colorimetric assay to measure released phosphate. (C) The activity of TEV-cleaved *At*DRP1A at various concentrations of GTP was used to calculate the kCat and kM for *At*DRP1A.

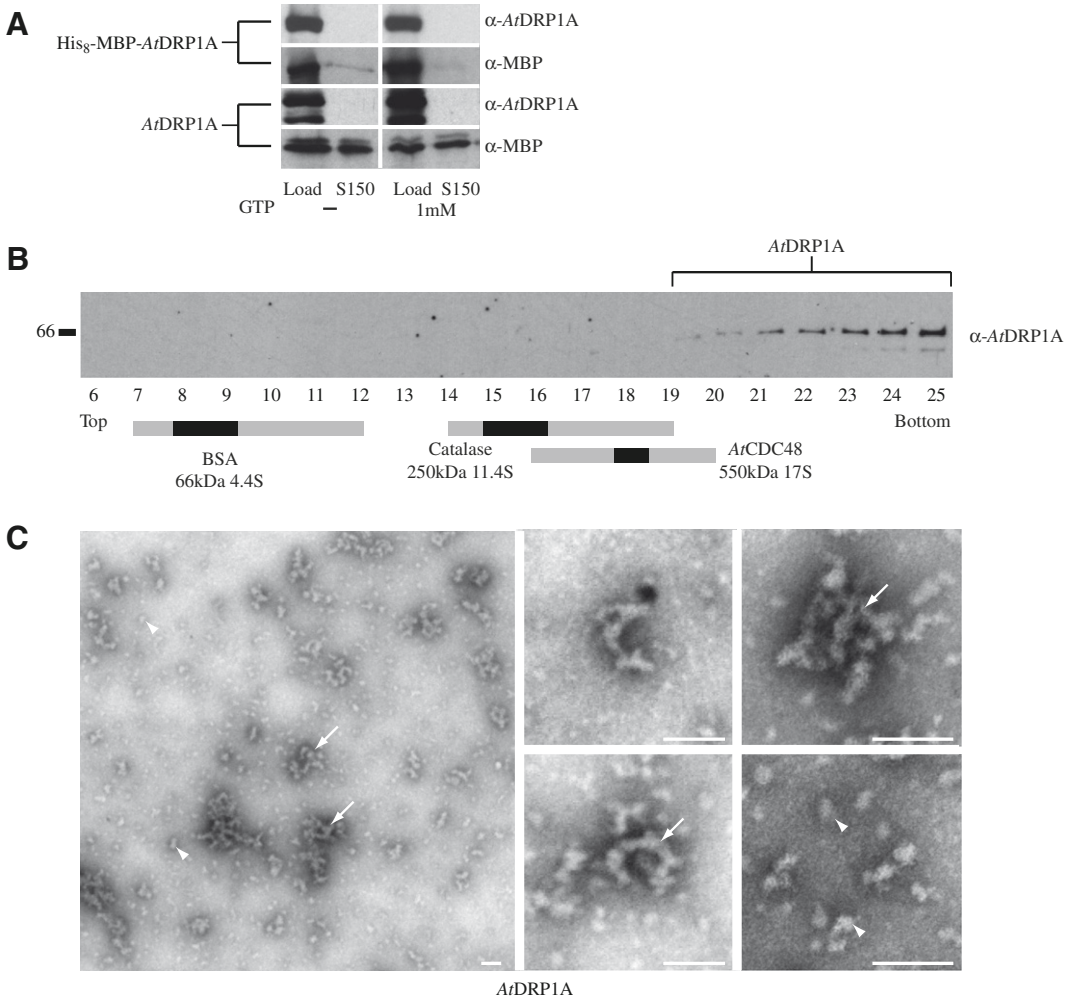

Fig. 2. *At*DRP1A forms large polymers *in vitro*. (A) Purified His_8-MBP -*At*DRP1A and TEV-cleaved *At*DRP1A (200 nM) was centrifuged at 150,000*g* in a pH 7.5 HEPES buffer containing 150 mM NaCl and 2 mM $MgCl_2$. The load and supernatant (S150) were analyzed by immunoblotting with antibodies against *At*DRP1A and MBP. The immunoblot was overexposed to demonstrate absence of AtDRP1A in the S150. (B) *At*DRP1A (50 nM) was separated on a 5–50% (w/v) sucrose gradient by centrifugation at 150,000*g* for 18 h and gradient fractions were analyzed by immunoblotting with antibodies against *At*DRP1A. Black and gray bars represent the peak and range, respectively, for three molecular weight markers (BSA 4.4S, Catalase 11.4S and AtCDC48 17S) run in parallel on a separate gradient and detected by SDS–PAGE gel analysis and Coomassie staining. Equivalent fractions were determined by measurement of refractive index. (C) *At*DRP1A (1 μM) visualized by electron microscopy after negative staining with Nano-W®. Right panels are higher magnification views. Arrowheads indicate smaller *At*DRP1A polymers; arrows indicate larger *At*DRP1A polymers. Scale bars = 100 nm.

(SMART server http://smart.embl-heidelberg.de/ [25]). Therefore, we examined whether or not *At*DRP1A polymers had any intrinsic affinity for PM phospholipids through binding studies to protein-free PM-mimetic (PMM) liposomes, whose lipid composition closely resembled that of the cytosolic face of the plant PM bilayer. Previous studies have determined the total lipid composition of the *Arabidopsis* PM [26] and have shown that PS is restricted to the inner leaflet of plant cell PMs [27]. PMM liposomes were generated from a mixture of 40 mol% β-sitosterol, 25 mol% Soy PC, 20 mol% DOPE, 10 mol% DOPS and 5 mol% DOPG with trace amounts of H^3-DOPC. Binding was assayed by liposome flotation followed by scintillation counting and immunoblotting. *At*DRP1A, but not His_8-MBP, showed robust binding to PMM liposomes (Fig. 3A).

The PMM liposomes have a net negative charge due to the presence of DOPS and DOPG, suggesting that the interaction with polymers of *At*DRP1A, which is predicted to have a net positive charge (PI = 8.5), might be based on charge–charge interactions. Consistent with this, *At*DRP1A did not show binding to uncharged liposomes lacking DOPS and DOPG (40 mol% β-sitosterol, 40 mol% Soy PC, 20 mol% DOPE) (Fig. 3B).

Interestingly, in spotted lipid overlay assays *At*DRP1A did not show binding to DOPS, but instead showed specific binding to PI(3)P and PI(5)P, with less binding to PI(4)P, similar to what has been reported for *At*DRP2A [28] (Supplementary Fig. 2A). However, in liposome flotation assays *At*DRP1A showed similar binding to DOPC-based liposomes containing 20% DOPS or 10% PI(3)P, PI(4)P or PI(5)P, as well as liposomes containing as little as 2% DOPS (Supplementary Fig. 2B–C).

AtDRP1A-induced liposome clustering

Both dynamin and the yeast dynamin-related protein *Sc*DMN1 (involved in mitochondrial fission) have been shown to assemble onto the outer surface of liposomes *in vitro*, and cause the deformation of those liposomes into tubules [29–34]. To determine whether *At*DRP1A polymers similarly affect liposome structure, protein-free PMM liposomes (Fig. 3B) and PMM liposomes preincubated with *At*DRP1A (Fig. 3C) were stained and visualized by EM. Liposomes bound to *At*DRP1A appeared as darkly staining clusters, which were not observed in protein-free liposome samples. The addition of GTP to these *At*DRP1A-liposome complexes resulted

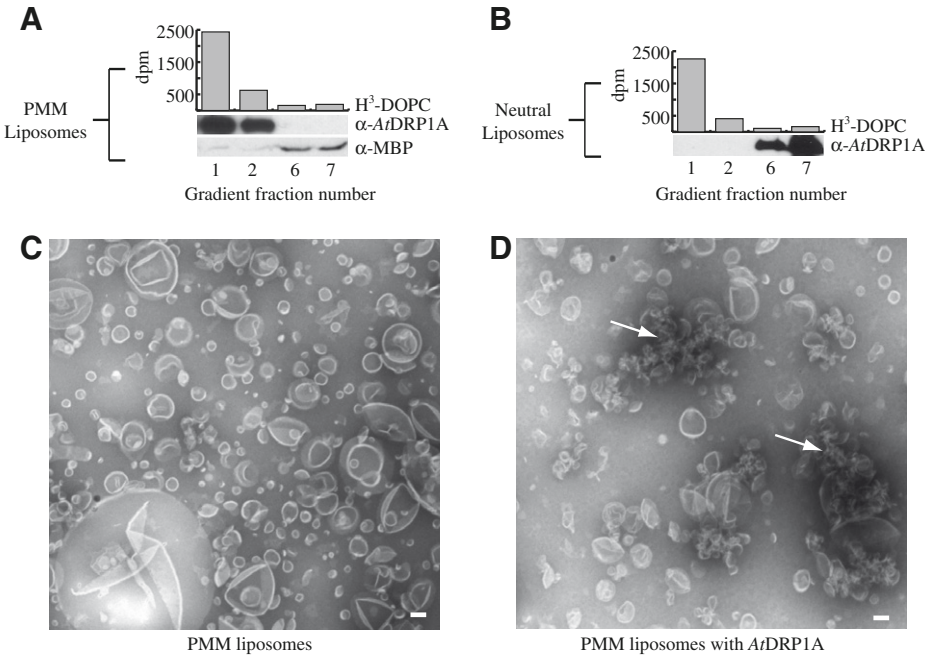

Fig. 3. *At*DRP1A binds and clusters protein-free liposomes. (A–B) Liposome flotation assay. (A) Arabidopsis Plasma Membrane Mimetic liposomes ("PMM": 40% β-sisterol, 25% Soy PC, 20% DOPE, 10%DOPS and 5% DOPG) or (B) neutrally charged liposomes ("Neutral": 40% β-sisterol, 40% Soy PC, 20% DOPE) spiked with trace H^3-DOPC were generated by extrusion through a 50 nm membrane. These liposomes (44 mM) were incubated with purified *At*DRP1A (250 nM) and separated from the load by flotation on a 40–30–0% (w/v) Accudenz step-gradient. The two top (1, 2) and the two bottom (6, 7) fractions of the gradient were analyzed by scintillation counting and immunoblotting with antibodies against *At*DRP1A and MBP. (C) PMM liposomes were stained with OsO_4 followed by Nano-W® and visualized by electron microscopy. (D) PMM liposomes were incubated with *At*DRP1A then stained and visualized as in (C). Arrows indicate clusters of liposomes induced by binding of *At*DRP1A. Scale bars in (C–D) = 100 nm.

in no discernible change in structure (Supplementary Fig. 3). This clustering of liposomes onto *At*DRP1A polymers is very different than what has been observed for dynamin or *Sc*DMN1 *in vitro*, and is also distinct from the *At*DRP1A-containing rings observed encircling cell plate membrane tubules *in vivo* during syncytial endosperm cellularization [6].

Conclusions

Our analysis of the *in vitro* structure and membrane lipid interaction of purified, bacterially-expressed *At*DRP1A suggest that the plant-specific DRP1 family has distinct characteristics from animal dynamin, even though previous studies have demonstrated that *At*DRP1A, like dynamin, functions in CME [5]. Likewise, the propensity of purified *At*DRP1A to form stable, GTP-insensitive, heterogeneous polymers that promote liposome clustering contrasts with the *in vivo* observation that *At*DRP1A-GFP exists in a cytoplasmic (presumably soluble) pool [4], and that *At*DRP1A can polymerize around membrane tubules during cell plate formation [6]. This suggests that *E. coli* expressed *At*DRP1A, while GTPase active, is lacking one or more *in vivo* factors necessary for modulating the polymeric state of individual *At*DRP1A subunits, and thereby polymerizes inappropriately into a form that does not retain full functionality.

One possibility is that the activity and polymeric structure of *At*DRP1A is regulated by post-translational modification, such as phosphorylation. Park et al. [8] found approximately 10% of cellular *At*DRP1A to be soluble upon cell disruption, and reported that this soluble form migrated slightly slower on SDS–PAGE gels. This slower migration could be reversed by alkaline-phosphatase treatment, suggesting that the soluble form of *At*DRP1A is phosphorylated. These results, together with our observations that *E. coli* expressed *At*DRP1A, which lacks phosphorylation, forms stable polymers, point to the need for further study of native *At*DRP1A, in particular the identification of post-translational modifications and/or relevant interacting proteins. The ability of these putative modifications or interacting proteins to modulate the polymeric and membrane binding characteristics of purified *At*DRP1A will be a key step in understanding the targeting and regulation of the plant-specific DRP1 family.

Acknowledgments

We would like to thank Dr. Tom Martin of the UW Madison Department of Biochemistry and members of his lab, including Judith Kowalchyk and Kristin Boswell, for their extensive help and advice with the lipid biding assays, and Randall Massey and Ben August of the UW Medical School EM facility for their help with the EM. We would like to thank Catherine Konopka and Brian Duerst for help with the generation of pVP16-TEV-DRP1A. We also thank current and former members of our lab, including David Rancour, Colleen McMichael and Sookhee Park for helpful discussions. This research was supported by funding to SYB from the USDA National Research Initiative Competitive Grants Program (project #2004-03411). SKB was supported by a National Institutes of Health, National Research Service Award T32 GM07215 from the National Institute of General Medical Sciences.

Appendix A. Supplementary data

Supplementary data associated with this article can be found, in the online version, at doi:10.1016/j.bbrc.2010.02.070.

References

[1] D.A. Collings, L.K. Gebbie, P.A. Howles, U.A. Hurley, R.J. Birch, A.H. Cork, C.H. Hocart, T. Arioli, R.E. Williamson, Arabidopsis dynamin-like protein DRP1A: a null mutant with widespread defects in endocytosis, cellulose synthesis, cytokinesis, and cell expansion, J. Exp. Bot. 59 (2008) 361–376.

[2] S. Sawa, K. Koizumi, S. Naramoto, T. Demura, T. Ueda, A. Nakano, H. Fukuda, *DRP1A* is responsible for vascular continuity synergistically working with *VAN3* in arabidopsis, Plant Physiol. 138 (2005) 819–826.
[3] B.H. Kang, J.S. Busse, C. Dickey, D.M. Rancour, S.Y. Bednarek, The arabidopsis cell plate-associated dynamin-like protein, ADL1Ap, is required for multiple stages of plant growth and development, Plant Physiol. 126 (2001) 47–68.
[4] B.H. Kang, J.S. Busse, S.Y. Bednarek, Members of the arabidopsis dynamin-like gene family, ADL1, are essential for plant cytokinesis and polarized cell growth, Plant Cell 15 (2003) 899–913.
[5] C.A. Konopka, S.Y. Bednarek, Comparison of the dynamics and functional redundancy of the arabidopsis dynamin-related isoforms DRP1A and DRP1C during plant development, Plant Physiol. 147 (2008) 1590–1602.
[6] M.S. Otegui, D.N. Mastronarde, B.H. Kang, S.Y. Bednarek, L.A. Staehelin, Three-dimensional analysis of syncytial-type cell plates during endosperm cellularization visualized by high resolution electron tomography, Plant Cell 13 (2001) 2033–2051.
[7] M. Mettlen, T. Pucadyil, R. Ramachandran, S.L. Schmid, Dissecting dynamin's role in clathrin-mediated endocytosis, Biochem. Soc. Trans. 37 (2009) 1022–1026.
[8] J.M. Park, S.G. Kang, K.T. Pih, H.J. Jang, H.L. Piao, H.W. Yoon, M.J. Cho, I. Hwang, A dynamin-like protein, ADL1, is present in membranes as a high-molecular-mass complex in arabidopsis thaliana, Plant Physiol. 115 (1997) 763–771.
[9] Z. Zhang, Z. Hong, D.P. Verma, Phragmoplastin polymerizes into spiral coiled structures via intermolecular interaction of two self-assembly domains, J. Biol. Chem. 275 (2000) 8779–8784.
[10] S. Dowler, G. Kular, D.R. Alessi, Protein lipid overlay assay, Science's STKE 2002 (2002).
[11] New England Biolabs, Phusion™ site-directed mutagenesis kit manual F-541, 2008.
[12] P.G. Blommel, B.G. Fox, A combined approach to improving large-scale production of tobacco etch virus protease, Protein Exprs. Purif. 55 (2007) 53–68.
[13] M. Leonard, B.D. Song, R. Ramachandran, S.L. Schmid, Robust colorimetric assays for dynamin's basal and stimulated GTPase activities, Methods Enzymol. 404 (2005) 490–503.
[14] D.M. Rancour, C.E. Dickey, S. Park, S.Y. Bednarek, Characterization of AtCDC48: evidence for multiple membrane fusion mechanisms at the plane of cell division in plants, Plant Physiol. 130 (2002) 1241–1253.
[15] W.C. Tucker, T. Weber, E.R. Chapman, Reconstitution of Ca2-regulated membrane fusion by synaptotagmin and SNAREs, Science 304 (2004) 435–438.
[16] B. Marks, M.H. Stowell, Y. Vallis, I.G. Mills, A. Gibson, C.R. Hopkins, H.T. McMahon, GTPase activity of dynamin and resulting conformation change are essential for endocytosis, Nature 410 (2001) 231–235.
[17] B.D. Song, M. Leonard, S.L. Schmid, Dynamin GTPase domain mutants that differentially affect GTP binding, GTP hydrolysis, and clathrin-mediated endocytosis, J. Biol. Chem. 279 (2004) 40431–40436.
[18] D.E. Warnock, J.E. Hinshaw, S.L. Schmid, Dynamin self-assembly stimulates its GTPase activity, J. Biol. Chem. 271 (1996) 22310–22314.
[19] J.F. Eccleston, D.D. Binns, C.T. Davis, J.P. Albanesi, D.M. Jameson, Oligomerization and kinetic mechanism of the dynamin GTPase, Eur. Biophys. J. 31 (2002) 275–282.
[20] R. Ramachandran, M. Surka, J.S. Chappie, D.M. Fowler, T.R. Foss, B.D. Song, S.L. Schmid, The dynamin middle domain is critical for tetramerization and higher-order self-assembly, EMBO J. 26 (2007) 559–566.
[21] J.E. Hinshaw, S.L. Schmid, Dynamin self-assembles into rings suggesting a mechanism for coated vesicle budding, Nature 374 (1995) 190–192.
[22] J.F. Carr, J.E. Hinshaw, Dynamin assembles into spirals under physiological salt conditions upon the addition of GDP and γ-phosphate analogues, J. Biol. Chem. 272 (1997) 28030–28035.
[23] K. Salim, M. Bottomley, E. Querfurth, M. Zvelebil, I. Gout, R. Scaife, R. Margolis, R. Gigg, C. Smith, P. Driscoll, Distinct specificity in the recognition of phosphoinositides by the pleckstrin homology domains of dynamin and bruton's tyrosine kinase, EMBO J. 15 (1996) 6241–6250.
[24] M. Achiriloaie, B. Barylko, J.P. Albanesi, Essential role of the dynamin pleckstrin homology domain in receptor-mediated endocytosis, Mol. Cell. Biol. 19 (1999) 1410.
[25] I. Letunic, T. Doerks, P. Bork, SMART 6: recent updates and new developments, Nucleic Acids Res. 37 (2009) D229–D232.
[26] M. Uemura, R. Joseph, P. Steponkus, Cold acclimation of arabidopsis thaliana (effect on plasma membrane lipid composition and freeze-induced lesions), Plant Physiol. 109 (1995) 15–30.
[27] I.E.W. O'Brien, C.P.M. Reutelingsperger, K.M. Holdaway, Annexin-V and TUNEL use in monitoring the progression of apoptosis in plants, Cytometry 29 (1997) 28–33.
[28] S.H. Lee, J.B. Jin, J. Song, M.K. Min, D.S. Park, Y.W. Kim, I. Hwang, The intermolecular interaction between the PH domain and the C-terminal domain of arabidopsis dynamin-like 6 determines lipid binding specificity, J. Biol. Chem. 277 (2002) 31842–31849.
[29] S.M. Sweitzer, J.E. Hinshaw, Dynamin undergoes a GTP-dependent conformation change causing vesiculation, Cell 93 (1998) 1021–1029.
[30] P. Zhang, J.E. Hinshaw, Three-dimensional reconstruction of dynamin in the constricted state, Nat. Cell Biol. 3 (2001) 922–926.
[31] Y.J. Chen, P. Zhang, E.H. Egelman, J.E. Hinshaw, The stalk region of dynamin drives the constriction of dynamin tubes, Nat. Struct. Mol. Biol. 11 (2004) 574–575.
[32] M.H. Stowell, B. Marks, P. Wigge, H.T. McMahon, Nucleotide-dependent conformational changes in dynamin: evidence for a mechanochemical molecular spring, Nat. Cell Biol. 1 (1999) 27–32.
[33] D. Danino, K.H. Moon, J.E. Hinshaw, Rapid constriction of lipid bilayers by the mechanochemical enzyme dynamin, J. Struct. Biol. 147 (2004) 259–267.
[34] E. Ingerman, E.M. Perkins, M. Marino, J.A. Mears, J.M. McCaffery, J.E. Hinshaw, J. Nunnari, Dnm1 forms spirals that are structurally tailored to fit mitochondria, J. Cell Biol. 170 (2005) 1021–1027.